Int. J. Electrochem. Sci., 17 **(2022)** Article Number: 2212114, doi: 10.20964/2022.12.95

International Journal of
ELECTROCHEMICAL
SCIENCE
www.electrochemsci.org

A Novel Electrochemical Sensor Based on Conductive $Cu_3(HITP)_2$/electrochemical Reduced Graphene Oxide Nanocomposite for Simultaneous Determination of Dopamine and Acetaminophen

Shanshan Li[1], *Hongxia Dai*[1,2,*], *Hui Chen*[1], *Jian Zhang*[1,*], *Xiaoning Shi*[1], *Haobo Zhang*[1]

[1] College of pharmacy, Gansu University of Chinese Medicine, Lanzhou, 730000, China
[2] Northwest Collaborative Innovation Center for Traditional Chinese Medicine Co-constructed by Gansu Province & MOE of PRC, Lanzhou, 730000, China
[*]E-mail: daihongxia007@163.com, zhangjian@gszy.edu.cn

Received: 14 November 2022 / *Accepted:* 12 December 2022 / *Published:* 27 December 2022

Monitoring small amount of dopamine (DA) and acetaminophen (ACOP) in biological samples is of great significance for the early prevention of neurological diseases and safe use of medicines in clinical research. A novel electrochemical sensor based on conductive metal organic framework $Cu_3(HITP)_2$ (HITP=2,3,6,7,10,11-hexaiminotriphenylene) and electrochemical reduced graphene oxide nanocomposite (denoted as $Cu_3(HITP)_2$/ERGO) was designed for simultaneous determination of DA and ACOP with enhanced sensitivity and selectivity. The $Cu_3(HITP)_2$/ERGO nanocomposite was characterized by scanning electron microcopy, energy dispersive spectroscopy and Fourier infrared spectroscopy. The oxidation potential separation of DA and ACOP achieved 226 mV. The $Cu_3(HITP)_2$/ERGO/GCE exhibited excellent electrochemical response towards the oxidation of DA and ACOP due to the superior conductivity and synergistic catalytic activity of $Cu_3(HITP)_2$/ERGO nanocomposite. The detection limits were 9 nM and 14 nM (S/N=3) for DA and ACOP with wide linear range of 0.05-150 μM and 0.1-100 μM, respectively. Furthermore, the proposed sensor has been successfully applied in the simultaneous detection of DA and ACOP in serum sample.

Keywords: $Cu_3(HITP)_2$; Electrochemical reduced graphene oxide; Electrochemical sensor; Dopamine; Acetaminophen.

1. INTRODUCTION

Dopamine (DA) and acetaminophen (ACOP) are nitrogen aromatic compounds with similar structure and electrochemical properties, which have been widely used in the pharmaceutical industry because of their good biological activities. DA-is an important biological catecholamine neurotransmitter

and plays a significant role in the mammalian-central nervous system [1]. The abnormal concentration of DA is associated with Parkinson's disease, schizophrenia, HIV infection and other neurological diseases [2]. ACOP, also known as paracetamol, is the most common and widely used antipyretic and analgesic drug in clinical practice, which can be used to relieve and treat toothache, headache and other symptoms [3]. However, long-term or excessive use of ACOP can cause many side effects such as nausea, anorexia, abdominal pain and even life-threatening. Besides, DA and ACOP often coexist and interfere with each other in biological samples [4]. Therefore, it is of great significance in clinical medicine and pharmacology to establish a rapid, accurate and sensitive method for the simultaneous detection of DA and ACOP. Since both DA and ACOP are electroactive molecules, their determination can be achieved by electrochemical method [5]. However, the discrimination of DA in the presence of ACOP is of great challenge, because of its overlapping oxidation peak potentials, poor stability and low sensitivity at the conventional electrodes [6]. In the past decades, several nanomaterials have been reported for modifying electrode surfaces, such as conductive polymers, carbon-derived materials, metal-organic frameworks, and metal and metal oxide nanoparticles [7].

Metal organic frameworks (MOFs), known as ordered porous materials composed of metal cluster nodes and organic bridging linkers, have attracted widespread attention in the electrochemical field [8–9]. The major problem of these MOFs is their low conductivity due to the high energy barrier of charge transfer and the limitation of free carriers [10]. So far, the research effort was mostly devoted to porous MOF substrates encapsulating conductive additives or annealed co-doped electrocatalysts [6, 11]. There are few reports on the construction of electrochemical sensors using self-conducting MOFs. In recent years, the emergence of conductive MOFs provides new opportunities for the application of MOFs in the field of electrochemistry [12]. In particular, the two-dimensional layered conducting MOFs, which consist of metal nodes (Cu or Ni) interlinked with organic ligands (2,3,6,7,10,11-hexahydroxytriphenylene, HHTP or 2,3,6,7,10,11- hexaiminotriphenylene, HITP), are very attractive in electrochemical sensing applications. Dincă et al. applied to the chemical resistive gas sensor for the first time. The conductivity of the two-probe method was 0.2 S cm^{-1} with the detection limit of 0.5 ppm for NH_3 [13]. Recently, Katherine et al. expanded the application of MOF in the field of electrochemical sensing by constructing an electrochemical sensor using a series of two-dimensional layered conducting MOFs for the selective determination of active neurochemicals [14]. However, the analytical performances of those sensors need to be further improved to meet the demand of trace components analysis in practical samples.

In this paper, the conductive Cu-based MOF ($Cu_3(HITP)_2$) was firstly combined with graphene oxide (GO), which is then converted to reduced graphene oxide (ERGO) by electrochemical reduction. The $Cu_3(HITP)_2$/ERGO modified electrode exhibited excellent electrochemical response towards the detection of DA and ACOP due to the superior conductivity and synergistic catalytic activity between $Cu_3(HITP)_2$ and ERGO. The proposed sensor with enhanced sensitivity and selectivity has been applied to detect DA and ACOP in serum sample, which provides a good application prospect in clinical research.

2. EXPERIMENTAL

2.1 Chemicals and apparatus

High purity graphite powder (>99.6%, 325 mesh) was purchased from Sigma Company in the United States. Triphenylene-2,3,6,7,10,11-hexaamino hydrochloride (HATP·6HCl) was from Shanghai TengQian Biotechnology Co., Ltd. Dopamine hydrochloride, acetamidophenol, potassium ferricyanide and potassium ferrocyanide were from Shanghai Aladdin Reagent Co., Ltd. Phosphate buffer solutions (PBS, 0.1M) were prepared by NaH_2PO_4-Na_2HPO_4 in the pH range of 5.0-7.0. All other chemicals were of analytical grade without further purification. All solutions were prepared with ultrapure water (18.25 MΩ cm).

The morphology and elemental composition of electrode surface materials were characterized by field emission scanning electron microscope (FESEM, S-4800, Japan) and energy dispersive X-Ray spectroscopy (EDS, JSM-5600LV, Japan), respectively. The structure of samples was confirmed by infrared spectroscopy (FTIR, Nicolet 6700, USA). All electrochemical measurements were performed on a CHI760E electrochemical workstation (Shanghai Chenhua Instrument Company, China). A platinum wire electrode, a saturated Ag/AgCl electrode and a bare or modified glassy carbon electrode (GCE, 3mm) were served as the auxiliary, reference, and the working electrodes, respectively.

2.2 Synthesis of $Cu_3(HITP)_2$ and $Cu_3(HITP)_2$/GO nanocomposites

Graphene oxide (GO) was prepared by improved Hummers′ method [15]. The conductive $Cu_3(HITP)_2$ was synthesized according to the reported literature with a minor alteration [13]: Briefly, 1.2 mL of ammonia solution and 20 mL of HATP·6HCl solution (0.074 mM) were added sequentially to 20 mL of $CuSO_4·5H_2O$ solution (0.11 mM). The resulted mixture was stirred for 30 s, and then stand at 25 ℃ for 3 hours to obtain the black suspension. Subsequently, the black suspension was centrifuged, and the precipitation was re-dispersed into 40 mL of water, followed by stirring continuously for 12 hours to remove impurities. Finally, the $Cu_3(HITP)_2$ precipitate was washed with acetone and dried under vacuum for 6 hours. After then, 1.0 mg of $Cu_3(HITP)_2$ was mixed with GO solution (1 mg mL^{-1}, 1 mL), and the mixture solution were ultrasonicated (200 W) for 30 min to form a homogeneous dispersion solution of $Cu_3(HITP)_2$/GO nanocomposite.

2.3 Fabrication of $Cu_3(HITP)_2$/ERGO modified electrode

6 μL of $Cu_3(HITP)_2$/GO suspension was deposited on a clean GCE and dried at room temperature (denoted as $Cu_3(HITP)_2$/GO/GCE). Then, $Cu_3(HITP)_2$/ERGO/GCE was fabricated by electrochemical reduction of $Cu_3(HITP)_2$/GO/GCE in 0.1 M PBS (pH 6.0) via cyclic voltammetry. The working conditions were as follows: potential range of −1.2 to +0.4 V with a scan rate of 100 mV s^{-1}, and number of cycles of 20.

2.4 Real sample preparation

Human whole blood samples were provided by the Affiliated Hospital of Gansu University of Traditional Chinese Medicine. After centrifugation, the supernatant was filtered by 0.45 μm filter membrane and diluted 100 times with 0.1 M PBS (pH 6.0). High pure N_2 gas was purged into the solution for 20 minutes before testing.

3. RESULTS AND DISCUSSION

3.1 Characterization of $Cu_3(HITP)_2$/ERGO nanocomposite

The morphological character of electrodes modified with as-synthesized $Cu_3(HITP)_2$/GO and $Cu_3(HITP)_2$/ERGO were characterized by SEM.

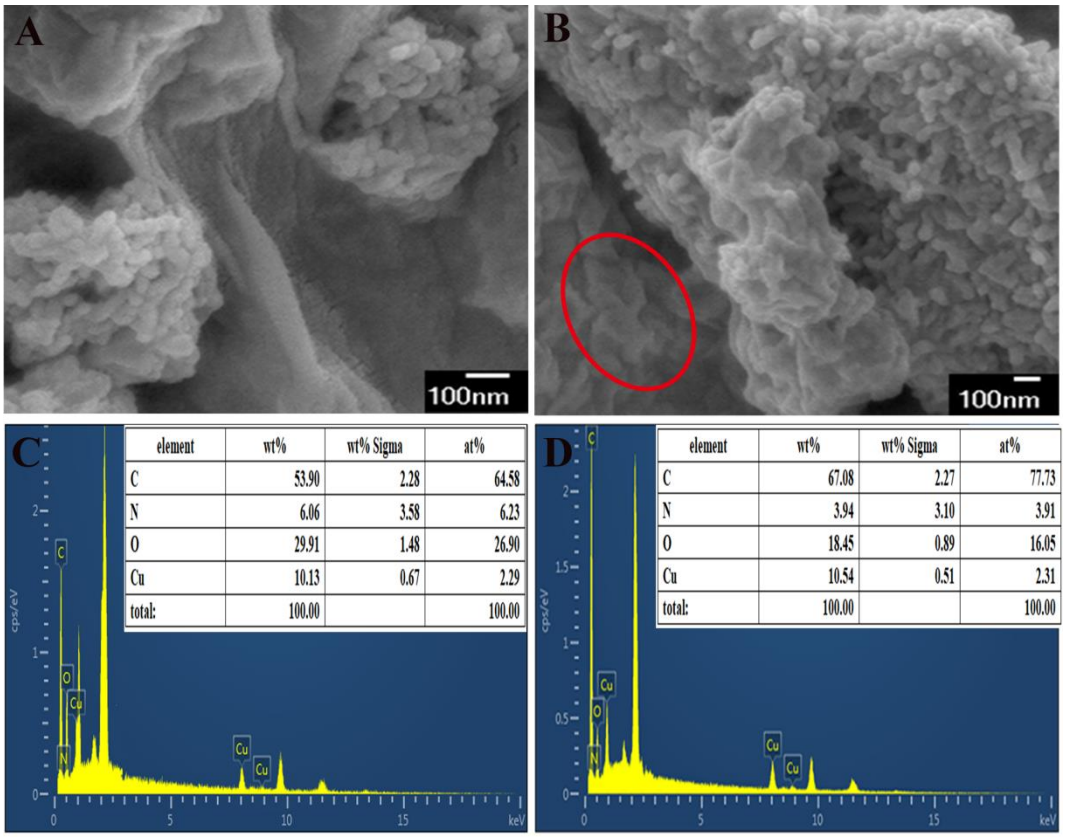

Figure 1. SEM images (A, B) and the corresponding EDS spectra (C, D) of electrodes modified with nanomaterials of $Cu_3(HITP)_2$/GO (A, C) and $Cu_3(HITP)_2$/ERGO (B, D). Insert: Table of corresponding element percentage content.

After hybridization with GO, $Cu_3(HITP)_2$ was wrapped by a wrinkled GO layer and remained its original rod-like structure (Figure 1A), which was consistent with the reported MOF/GO characteristics [16]. After electrochemical reduction of GO to ERGO, the rod-like $Cu_3(HITP)_2$ was still encapsulated

by ERGO, but the surface of $Cu_3(HITP)_2$/ERGO/GCE was rougher with random wrinkles than that of $Cu_3(HITP)_2$/GO/GCE (Figure 1B). The elements in the composites were identified by EDS spectroscopy. As shown in Figure 1C and 1D, the corresponding oxygen content of $Cu_3(HITP)_2$/ERGO was reduced to 18.45% compared to 29.91% of $Cu_3(HITP)_2$/GO, verifying the successful conversion of GO to ERGO in the nanocomposite.

The interaction between $Cu_3(HITP)_2$ and ERGO was studied by FT-IR spectroscopy. As seen in Figure 2A, the characteristic bands of $Cu_3(HITP)_2$ (curve a) at 3434, 1617, 1351, 883 cm^{-1} were assigned to the stretching vibrations of N–H, C=C, C–N and N–Cu–N in $Cu_3(HITP)_2$ [17–18]. As for $Cu_3(HITP)_2$/GO (curve b), the peaks at 3448 and 1708 cm^{-1} correspond to the O–H and C=O stretching vibrations in GO. Compared with GO (curve c), it was found that the peaks of C=O bands of $Cu_3(HITP)_2$/GO shifted from 1728 to 1708 cm^{-1}, indicating the π-π interactions between GO and $Cu_3(HITP)_2$ [19]. Moreover, the peak intensity of $Cu_3(HITP)_2$/ERGO corresponding to oxygen-containing functional groups (~3440 and 1052 cm^{-1}) decreased or disappeared in different degrees (curve d), once again verifying the successful conversion of GO to ERGO in the nanocomposite.

The charge transport and conductivity of different electrode surfaces were evaluated by electrochemical impedance spectroscopy (EIS). Figure 2B showed the EIS spectra of bare GCE and different modified electrodes. The impedance data obtained were best fitted with equivalent circuit model (inset of Figure 2B). The semicircular part of Nyquist's diagram is related to the charge transfer impedance (R_{ct}). The R_{ct} value of $Cu_3(HITP)_2$/GCE was 208 Ω (curve b), which was smaller than that of bare GCE (316 Ω, curve a), illustrating the good intrinsic conductivity of $Cu_3(HITP)_2$. However, the poor conductivity of GO increased the R_{ct} value of $Cu_3(HITP)_2$/GO/GCE to 488 Ω (curve c). After electrochemical reduction of $Cu_3(HITP)_2$/GO, the semicircle diameter (curve d) notably decreased compared to $Cu_3(HITP)_2$/GO/GCE. The R_{ct} value of $Cu_3(HITP)_2$/ERGO/GCE was as low as 20 Ω, indicating that the electrochemical reduction of graphite oxide could significantly accelerate the charge transfer rate, and thus improving the electrochemical performance of $Cu_3(HITP)_2$/ERGO/GCE.

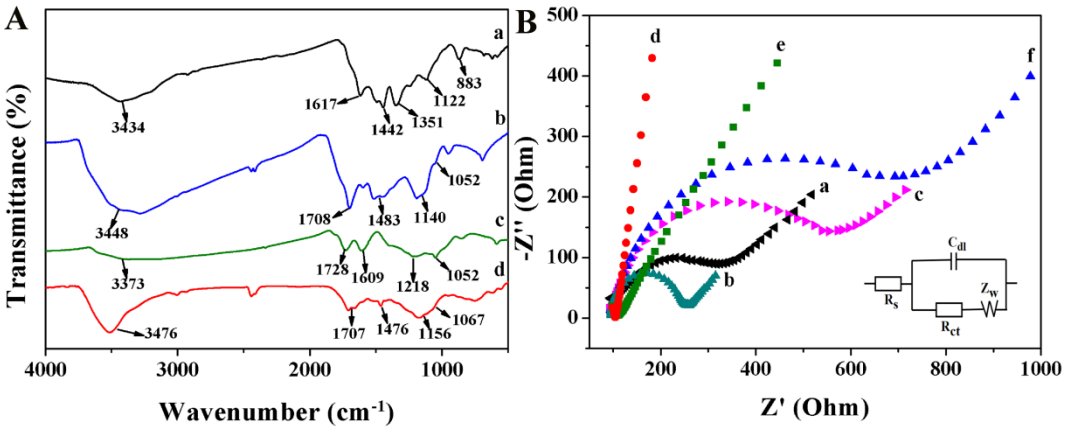

Figure 2. (A) FTIR spectrograms of $Cu_3(HITP)_2$ (a), $Cu_3(HITP)_2$/GO (b), GO (c) and $Cu_3(HITP)_2$/ERGO (d). (B) EIS curves of bare GCE (a), $Cu_3(HITP)_2$/GCE (b), $Cu_3(HITP)_2$/GO/GCE (c), $Cu_3(HITP)_2$/ERGO/GCE (d), ERGO/GCE (e) and GO/GCE (f) in 5.0 mM $[Fe(CN)_6]^{3-/4-}$ solution. Insert: Randle equivalent electrical circuit.

3.2 Electrochemical behavior of DA and ACOP at $Cu_3(HITP)_2$/ERGO/GCE

In order to investigate the electrochemical sensing performance of $Cu_3(HITP)_2$/ERGO/GCE, cyclic voltammetry (CV) was used to record the electrochemical response of different electrodes to-10 μM DA and 20 μM ACOP at scan rate of 50 mV s^{-1} in 0.1 M PBS (pH 6.0). As displayed in Figure 3, there were broad peak with weak peak currents for DA and ACOP were observed at the bare GCE. It was clear seen that the electrochemical reaction of these two species at the bare GCE were irreversible and underwent sluggish electron transfer kinetic process. After the modification of GO on the GCE, the corresponding peak current increased and the reversibility of DA improved (redox peak potential difference ΔE_p=192 mV), due to the excellent electrocatalytic activity of GO. Compared to GO/GCE, $Cu_3(HITP)_2$/GO/GCE could separate the oxidation peak of DA and ACOP more effectively. The ΔE_p value of DA decreased to 86 mV with the increase of peak current, indicating a better reversibility of DA at $Cu_3(HITP)_2$/GO/GCE, which were consistent with the good electrocatalytic activity and conductivity of $Cu_3(HITP)_2$. Moreover, the oxidation peak potential of DA and ACOP moved negatively to 0.25 and 0.46 V, respectively. Lower overpotentials demonstrated the existence of synergy between $Cu_3(HITP)_2$ and GO. Notably, two well-defined redox peaks of DA and ACOP were obtained at $Cu_3(HITP)_2$/ERGO/GCE after GO was electrochemical reduced. The ΔE_p value of DA and ACOP decreased to 58 mV and 72 mV, suggesting a reversible electrochemical reaction occurred on the electrode. Besides, the oxidation peak currents of DA and ACOP increased sharply to 23.99 μA and 21.79 μA at $Cu_3(HITP)_2$/ERGO/GCE, which were 25-times of bare GCE, 6-times of GO/GCE, and 4-times of $Cu_3(HITP)_2$/GO/GCE, respectively. The result verified that the conversion of GO to ERGO further enhanced the electrical conductivity of $Cu_3(HITP)_2$/ERGO/GCE, which showed high electrocatalytic activities for the oxidation of DA and ACOP. The difference of the oxidation peak potential between DA and ACOP was 226 mV, which ensured the simultaneous detection of DA and ACOP without mutual interference.

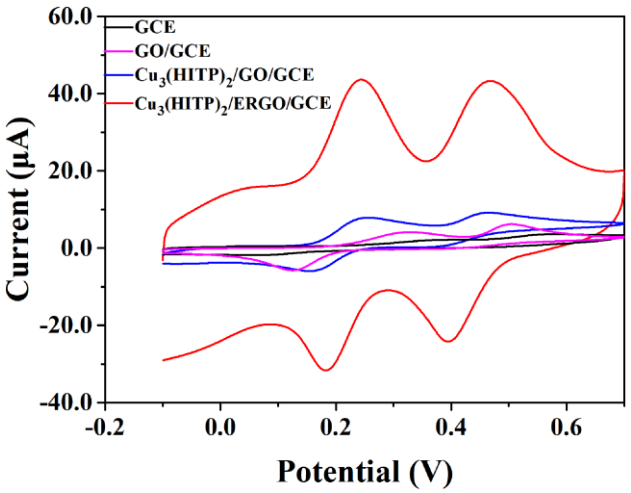

Figure 3. The CVs of GCE, GO/GCE, $Cu_3(HITP)_2$/GO/GCE and $Cu_3(HITP)_2$/ERGO/GCE in 0.1 M PBS (pH 6.0) containing the mixture of 10 μM DA and 20 μM ACOP at scan rate of 50 mV s^{-1}.

Figure 4A and 4B showed the CVs of DA and ACOP at $Cu_3(HITP)_2$/ERGO/GCE by changing the scan rate (v) from 20 to 250 mV s^{-1}. With the increase of scanning rate, the oxidation peak potential shifted positively, while the reduction peak potential shifted negatively. Moreover, the redox peak currents increased linearly with square root of the scan rate ($v^{1/2}$) (Figure 4C and 4D), indicating that the electrochemical kinetics of DA and ACOP at $Cu_3(HITP)_2$/ERGO/GCE was a typical diffusion-controlled process [20].

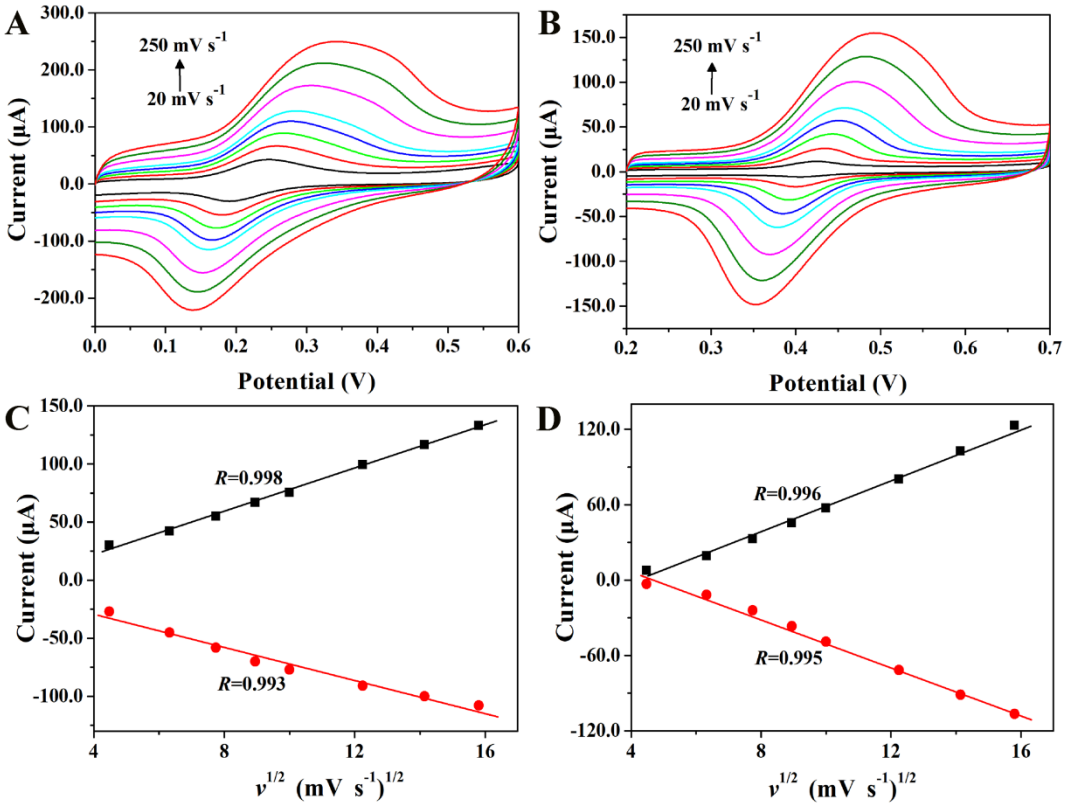

Figure 4. The CVs of $Cu_3(HITP)_2$/ERGO/GCE in 0.1 M PBS (pH 6.0) containing 20 μM DA (A) and 20 μM ACOP (B) with different scan rates (20-250 mV s^{-1}). Plots of the peak currents of DA (C) and ACOP (D) versus the square roots of the scan rates ($v^{1/2}$).

The effect of pH on the CV responses to 20 μM DA and ACOP at $Cu_3(HITP)_2$/ERGO/GCE was investigated in Figure 5. As the pH value increased from 5.0 to 7.0, the anodic peak potentials (E_{pa}) of DA and ACOP shifted negatively (Figure 5A and 5B). The linear slopes of the plots of E_{pa} versus the pH value were 63.6 and 65.6 mV pH^{-1} for DA and ACOP, respectively (Figure 5C). These slops were close to the expected Nernstian value of 59 mV pH^{-1} [21], suggesting that the electrooxidation reaction of DA and ACOP at $Cu_3(HITP)_2$/ERGO/GCE involved equal number of electrons and protons ($2e^-/2H^+$). The possible mechanism of electrochemical reaction of DA and ACOP can be expressed as follows (Scheme 1):

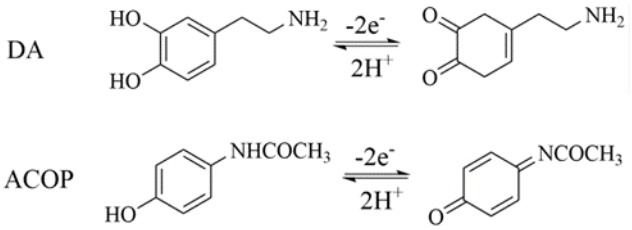

Scheme 1. A proposed electrode reaction mechanism for DA and ACOP at $Cu_3(HITP)_2$/ERGO/GCE

Moreover, as pH value changed from 5.0 to 6.0, the anodic peak currents of DA and ACOP increased gradually and then decreased sharply when pH was greater than 6.0 (Figure 5D). Thus, pH 6.0 was selected as the optimum solution pH for subsequent experiments to obtain higher sensitivity.

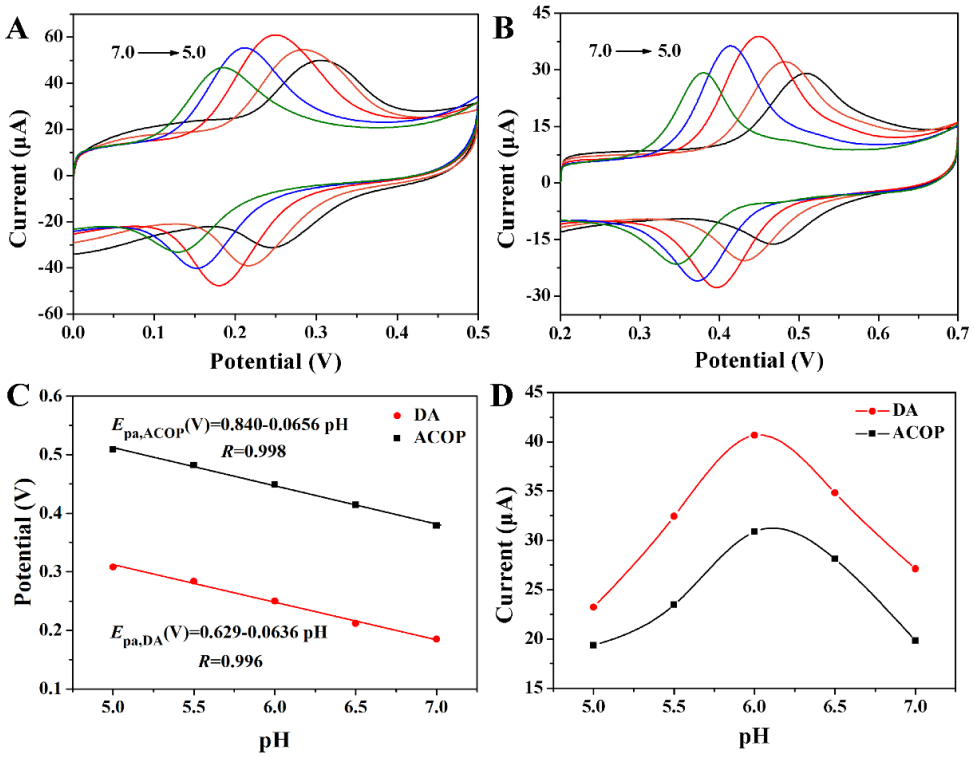

Figure 5. CVs of 20 μM DA (A) and 20 μM ACOP (B) at $Cu_3(HITP)_2$/ERGO/GCE with different pH (5.0-7.0). Effect of pH value on the anodic peak potential (C) and peak current (D) for DA and ACOP.

The electrocatalytic oxidation of DA and ACOP at $Cu_3(HITP)_2$/ERGO/GCE were also discussed by chronoamperometry (Figure 6). The diffusion coefficient (*D*) for DA and ACOP at $Cu_3(HITP)_2$/ERGO/GCE could be calculated by using Cottrell equation [22]:

$$I = nFAD^{1/2}c\pi^{-1/2}t^{-1/2}$$

where *n*, *A*, *D*, *c*, and *I* represent the total number of electrons transferred, effective surface area of the electrode (cm^2), the diffusion coefficient ($cm^2\ s^{-1}$), the concentration of analyte (mol mL^{-1}), and the peak current, respectively. According to the slopes of the *I* versus $t^{-1/2}$ plots (insets of Figure 6A and

6B), the D of DA and ACOP were 9.37×10^{-5} cm^2 s^{-1} and 5.66×10^{-5} cm^2 s^{-1}, respectively. Furthermore, the catalytic rate constant (k_{cat}) can be further calculated according to the following equation:

$$I_{cat}/I_L = \left(\pi k_{cat} ct\right)^{1/2}$$

Where I_{cat}, I_L and t represent the catalytic current of analyte at the surface of modified electrode, the limited current in the absence of analyte, respectively. From the slopes of the I_{cat}/I_L versus $t^{1/2}$ plots, the value of k_{cat} was evaluated to be 4.31×10^4 M^{-1} s^{-1} for DA and 7.94×10^4 M^{-1} s^{-1} for ACOP. These values for the catalytic rate constant of DA and ACOP oxidation was higher than values reported by some other works [23–25], suggesting a higher rate of the reaction.

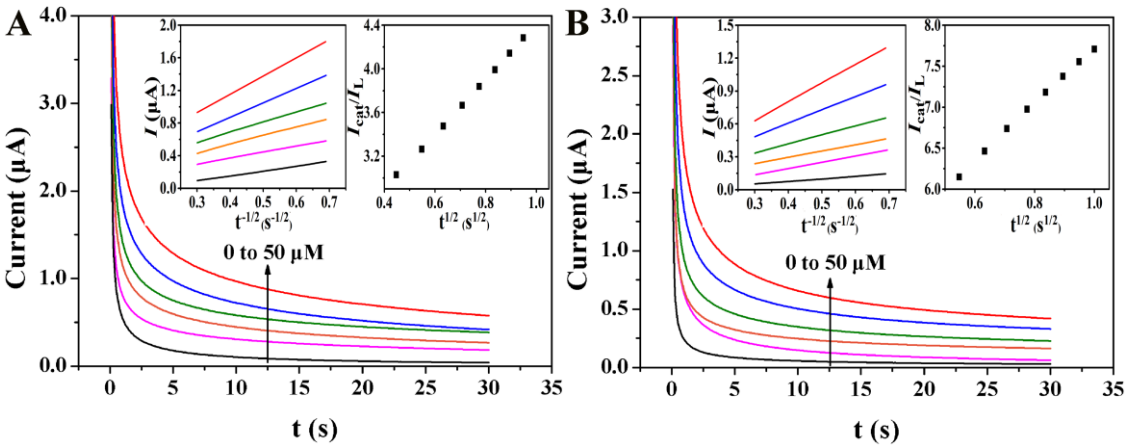

Figure 6. Chronoamperometric responses for varying concentrations of DA (A) and ACOP (B) at $Cu_3(HITP)_2$/ERGO/GCE in 0.1 M PBS (pH 6.0) in the concentration range of 0, 10, 20, 30, 40 and 50 μM. Inset: Plots of I vs. $t^{-1/2}$ for various concentrations of DA and ACOP and the plots of I_{cat}/I_L vs. $t^{1/2}$ obtained from the chronoamperograms, respectively.

3.3 Individual and simultaneous determination of DA and ACOP

Individual and simultaneous detection of DA and ACOP at $Cu_3(HITP)_2$/ERGO/GCE was performed by differential pulse voltammetry (DPV). In binary mixtures, individual determination of the two matters was explored by changing the concentration of one analyte while leaving the other unchanged (Figure 7A and 7C). The oxidation peak potential of DA and ACOP were located at +0.20 V and +0.41 V, respectively. In the case of ACOP coexistence, the peak current of DA increased linearly with the increase of concentration (Figure 7A). The linear regression equations of DA were I_p(μA) = 0.955 + 4.618 c (μM) (R^2=0.9985, 0.05-10 μM) and I_p(μA) = 45.845 + 0.495 c (μM) (R^2=0.9971, 10-150 μM) (Figure 7B). The trend of ACOP was similar to that of DA (Figure 7C), the linear regression equations were I_p(μA) = 2.242 + 3.455 c (μM) (R^2=0.9980, 0.1-10 μM) and I_p(μA) = 31.081 + 0.596 c (μM) (R^2=0.9976, 10-100 μM) (Figure 7D). The detection limits (S/N=3) for DA and ACOP were calculated as 9 nM and 14 nM, respectively. These results confirmed the higher sensitivity of the sensor based on $Cu_3(HITP)_2$/ERGO/GCE as compared the other sensors as listed in Table 1. This is mainly due

to the synergy between $Cu_3(HITP)_2$ and ERGO to form a large π-π conjugate system, which possesses sufficient active sites and excellent conductivity.

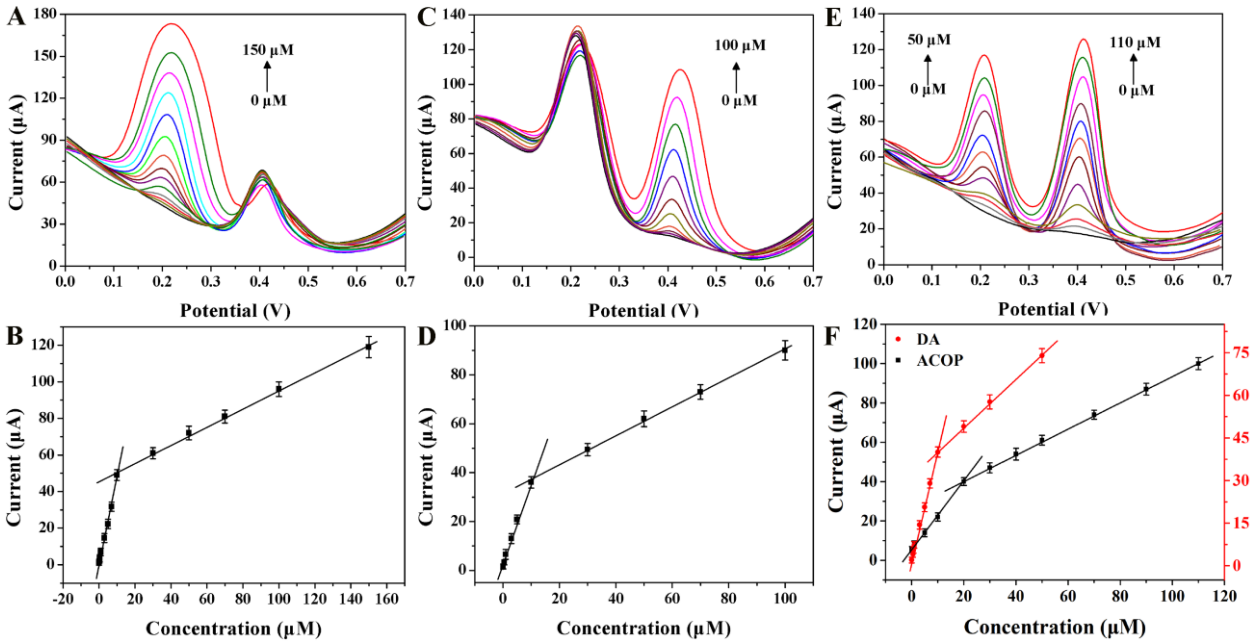

Figure 7. DPVs of the $Cu_3(HITP)_2$/ERGO/GCE in 0.1 M PBS (pH 6.0) containing DA (0-150 μM) and 30 μM ACOP (A), 70 μM DA and ACOP (0-100 μM) (C) and the mixture of various concentrations of DA (0-50 μM) and ACOP (0-110 μM) (E). The corresponding linear relationships between the oxidation peak currents and concentrations of DA (B), ACOP (D) in A and C, and the corresponding calibration curves of DA and ACOP in E (F).

Table 1. Comparisons of the performances of modified electrodes for the simultaneous detection of DA and ACOP.

Modified materials [a]	Linear range (μM)		Detection limit (μM)		Refs.
	DA	ACOP	DA	ACOP	
Cu-MOFs/MWCNT-Au@Ag	0.6-70	1.0-40	0.083	0.232	6
	70-300	40-500			
HKUST-1/ERGO	0.2-300	0.2-160	0.013	0.016	11
$Cu_3(HITP)_2$	—	—	2.3	—	14
ZIF-67	2-22	2-22	1.3	1.4	26
Cu(tpa)-EGR	1-50	1-100	0.21	0.36	27
$CoFe_2O_4$/GP	3-180	3-200	0.35	0.25	28
TAPT-TFP-COF/COOH-MWCNT	1-190	1-190	0.14	0.19	29
AG-NA	0.5-35	0.05-20	0.33	0.031	30
$Cu_3(HITP)_2$/ERGO	0.05-10	0.1-10	0.009	0.014	This work
	10-150	10-100			

[a] GP: graphite; TAPT: 1,3,5-tris-(4-aminophenyl) triazine; TFP: 1,3,5-triformyl phloroglucinol; AG: activated graphene; NA: Nafion.

Compared with the individual determination, the simultaneous determination of multiple components is more universal. Thus, the feasibility of the simultaneous detection of DA and ACOP based on $Cu_3(HITP)_2$/ERGO/GCE was studied by changing the concentrations of two components simultaneously (Figure 7E). The proposed sensor still exhibited two segments of linearity for DA and ACOP (Figure 7F). The linear regression equations were I_p(μA) = 2.614 + 3.742 *c* (μM) (R^2=0.9990, 0.05-10 μM) and I_p(μA) = 31.863 + 0.848 *c* (μM) (R^2=0.9982, 10-50 μM) with the detection limit of 11 nM (S/N=3) for DA. As for ACOP, the linear regression equations were I_p(μA) = 5.592 + 1.705 *c* (μM) (R^2=0.9985, 0.1-20 μM) and I_p(μA) = 27.207 + 0.665 *c* (μM) (R^2=0.9992, 20-110 μM) with the detection limit of 26 nM. The two linear segments could be attributed to the dynamic behavior of the substrate on the electrode surface. At low concentration levels, the substrate is quickly catalyzed by $Cu_3(HITP)_2$/ERGO composite, and the local concentration at the electrode surface is quickly consumed, resulting in high sensitivity. However, at high concentrations, it takes a longer time for the substrate to diffuse to the electrode surface, and the reaction products may foul the electrode surface, resulting in a lower sensitivity. It was noted that the sensing performance of $Cu_3(HITP)_2$/ERGO composite is better than that of other MOF/ERGO composites (such as HKUST-1/ERGO), which may be caused by the excellent conductivity of $Cu_3(HITP)_2$.

3.4 Selectivity, reproducibility and stability

In order to evaluate the selectivity of the developed sensor towards DA and ACOP, DPV measurements were carried out via the successive injection with DA, ACOP and various interfering substances such as common ions and compounds. It was found that the common inorganic ions (100-fold excess) such as Na^+, K^+, Cu^{2+}, Ca^{2+}, Cl^-, NO_3^-, some organic molecules (50-fold excess) including glucose, lactose, ascorbic acid, and uric acid, had little effect on determination of 5 μM DA and 30 μM ACOP. The changes of peak current were less than 10%, indicating good selectivity and anti-interference of the sensor. The reproducibility of the $Cu_3(HITP)_2$/ERGO/GCE was examined by six separately-prepared electrodes. The results revealed that the proposed sensor exhibited a satisfied reproducibility with relative standard deviations (RSD) of 1.8% for DA and 2.4% for ACOP. Stability tests were performed every 5 days in PBS containing 5 μM DA and 30 μM ACOP. After 30 days, the responses of DA and ACOP remained 91.2% and 92.7% of the initial current, indicating a satisfied stability of the developed sensor.

3.5 Real sample analysis

The reliability of the proposed $Cu_3(HITP)_2$/ERGO/GCE for the simultaneous sensing of DA and ACOP was performed in human serum samples by standard addition method. The serum samples were diluted with 0.1 M PBS (pH 6.0) with a ratio of 1:100. As shown in Table 2, the recoveries of added concentrations were varied from 96.4%-103.6% for DA and 96.0%-101.2% for ACOP, respectively. The RSDs of three parallel detections for each sample were less than 5.0%. Those results demonstrated that

the proposed sensor can be successfully applied to the simultaneous determination of DA and ACOP in biological samples.

Table 2. Recovery tests of DA and ACOP in human serum samples (*n*=3).

Analyte	Added (μM)	Found (μM)	Recovery (%)	RSD (%)
DA	5.0	4.9	98.0	3.9
	25.0	24.1	96.4	2.2
	50.0	51.8	103.6	3.5
ACOP	5.0	4.8	96.0	4.1
	25.0	25.3	101.2	3.2
	50.0	49.5	99.0	2.3

4. CONCLUSIONS

In summary, we successfully prepared a novel electrochemical sensor based on $Cu_3(HITP)_2$/ERGO/GCE with high sensitivity and selectivity for the detection of DA and ACOP. Compared with conventional MOF, $Cu_3(HITP)_2$ with intrinsic good conductivity could not only catalyze the oxidation of analyte but also accelerate the electron transfer at the electrode surface. The addition of GO strengthened the attachment of the modified material on the electrode surface and enhanced their stability. The electrochemical reduction of GO further promoted the synergistic effect between $Cu_3(HITP)_2$ and ERGO, which provided $Cu_3(HITP)_2$/ERGO/GCE with sufficient active sites and excellent conductivity. The proposed sensor exhibits lower detection limits and wider linear ranges, and has been successfully applied to simultaneous detection of DA and ACOP in human serum samples. The proposed method expands the application of conductive MOFs in multicomponent detection, and has a promising application prospect in clinical research.

ACKNOWLEDGMENTS
This work was supported by the National Natural Science Foundation of China (No. 21562001), the Educational Science and Technology Innovation Program of Gansu Province (No. 2021CYZC-13), the Natural Science Foundation of Gansu Province (No. 20JR10RA328), and the Young and Middle-aged Research Fund Project of Gansu University of Chinese Medicine (No. ZQ2017-11).

References

1. C.E. Grant, A. Flis, B.M. Ryan, *Carcinogenesis*, 43 (2022) 517.
2. X. Liu, J. Liu, *View*, 2 (2021) 20200102.
3. L. Wang, T. Meng, Y. Fan, C. Chen, Z. Guo, H. Wang, Y. Zhang, *J. Colloid Interface Sci.*, 524 (2018) 1.
4. S.P. Wilson, D.L. Kamin, J.M. Feldman, *Clin. Chem.*, 31 (1985) 1093.

5. B.J. Privett, J.H. Shin, M.H. Schoenfisch, *Anal. Chem.*, 82 (2010) 4723.
6. W. Yao, H. Guo, H Liu, Q. Li, R. Xue, N. Wu, L. Li, M. Wang, W. Yang, *J. Electrochem. Soc.*, 166 (2019) B1258.
7. S. Lakard, I.A. Pavel, B. Lakard, *Biosensors*, 11 (2021) 179.
8. T. Ma, H. Li, J.G Ma, *Dalton Trans.*, 49 (2020) 17121.
9. H. Dai, W. Lü, X. Zuo, Q. Zhu, C. Pan, X. Niu, J. Liu, H. Chen, X. Chen, *Biosens. Bioelectron.*, 95 (2017) 131.
10. G. Zhang, L. Jin, R. Zhang, *Coord. Chem. Rev.*, 439 (2021) 213915.
11. B. Ma, H. Guo, M. Wang, W. Yang, *Electroanalysis*, 31 (2019) 1002.
12. J. Liu, X. Song, T. Zhang, S. Liu, H. Wen, L. Chen, *Angew. Chem.*, 133 (2021) 5672.
13. M.G. Campbell, D. Sheberla, S.F. Liu, T.M. Swager, M. Dincă, *Angew. Chem., Int. Ed.*, 54 (2015) 4349.
14. M. Ko, L. Mendecki, A.M. Eagleton, C.G. Durbin, R.M. Stolz, Z. Meng, K.A. Mirica, *J. Am. Chem. Soc.*, 142 (2020) 11717.
15. W.S. Hummers, R.E. Offeman, *J. Am. Chem. Soc.*, 80 (1958) 1339.
16. N. Song, Y. Sun, X. Xie, *Desalination*, 492 (2020) 114601.
17. W. Wu, L. Zhan, W. Fan, J. Song, H. Zeng, *Angew. Chem., Int. Ed.*, 54 (2015) 6540.
18. Y. Ma, Y. Cen, M. Sohail, Q. Hu, *ACS Appl. Mater. Interfaces*, 9 (2017) 33011.
19. H. Wang, Q. Hao, X. Yang, L. Lu, X. Wang, *Electrochem. Commun.*, 11 (2009) 1158.
20. T. Iranmanesh, M.M Foroughi, S. Jahani, *Talanta*, 207 (2020) 120318.
21. A.S. Feiner, A. McEvoy, *J. Chem. Educ.*, 71 (1994) 493.
22. A. Yamada, Y. Kato, T. Yoshikuni, *Anal. Chim. Acta*, 112 (1979) 55.
23. N. Setoudeh, S. Jahani, M. Kazemipour, *J. Electroanal. Chem.*, 863 (2020) 114045.
24. Y. Kang, N. Shang, X. Lan, *Colloids Surf., A*, 641 (2022) 128620.
25. H. Yang, C. Zhou, J. An, *J. Alloys Compd.*, 897 (2022) 163257.
26. N.T.T. Tu, P.C. Sy, T.V. Thien, D.Q. Khieu, *J. Mater. Sci.*, 54 (2019) 11654.
27. X. Wang, Q. Wang, F. Gao, H. Guo, *ACS Appl. Mater. Interfaces*, 6 (2014) 11573.
28. Y. Kumar, P. Pramanik, D.K. Das, *Heliyon*, 5 (2019) e02031.
29. H. Guo, L. Sun, M. Yang, W. Yang, *Anal. Methods*, 13 (2021) 4994.
30. D. Kim, S. Lee, Y. Piao, *J. Electroanal. Chem.*, 794 (2017) 221.